The 2010 IEEE/RSJ International Conference on
Intelligent Robots and Systems
October 18-22, 2010, Taipei, Taiwan

Ball Dribbling with an Underactuated Continuous-Time Control Phase: Theory & Experiments

Georg Bätz, Uwe Mettin, Alexander Schmidts, Michael Scheint, Dirk Wollherr and Anton S. Shiriaev

Abstract— **Ball dribbling is a central element of basketball. One main challenge for realizing basketball robots is to stabilize periodic motion of the ball. The task is nontrivial due to the discrete-continuous nature of the corresponding dynamics. This paper proposes to add an elastic element to the manipulator so the ball can be controlled in a continuous-time phase instead of an intermittent contact. Optimal catching and pushing trajectories are planned for the underactuated system based on the virtual holonomic constraints approach. First experimental studies are presented to evaluate the approach.**

Index Terms - **Underactuated Mechanical System, Motion Planning, Orbital Stabilization, Virtual Holonomic Constraints**

I. INTRODUCTION

The control of periodic tasks has been an active research area over the last 25 years. The classical example is the so-called *juggling* that requires interaction with an object or multiple objects that would otherwise fall freely in the earths gravitational field [1]. These tasks generally constitute nontrivial dynamic environments and their dynamic properties change intermittently subject to excitation from the manipulator. For juggling tasks, the continuous motion of an actuator is used to control the continuous motion of the ball through an intermittent contact. Open-loop control of a vertically bouncing ball with repeated impacts has been studied in [2]. Orbital stabilization of juggling trajectories is discussed in [3], [4].

The *dribbling* task is, to some extent, comparable to the extensively studied *classic juggling* task. An example of robot dribbling was presented in [5] for experimental evaluation of a high-speed vision system. A comparison between juggling and dribbling is discussed in [6] with respect to local stability and parameter sensitivity. Furthermore, experimental results were shown with an industrial robot dribbling a basketball for multiple periods of a desired cycle.

The novelty of this paper is the evaluation of ball dribbling with a continuous-time control phase instead of an intermittent contact between manipulator and ball. The continuous-time control is realized by adding a mechanical spring element to the manipulator so that impacts are avoided when the ball bounces against it. Compared to the intermittent control, the novel approach offers two advantages: First, the control of the ball motion is facilitated. Over a significant time interval, the kinetic energy of the ball is converted to potential energy of the spring and eventually released back to the ball. During this time period, a controller can take stabilizing action. Second, by avoiding impacts between manipulator and ball the mechanical load for the manipulator is reduced.

The remainder of the paper is organized as follows: In Sec. II, a hybrid (discrete-continuous) system model is derived. A detailed description of the motion planning is given in Sec. III. The control design is presented in Sec. IV and experimental results are shown in Sec. V. Finally, a conclusion and outlook can be found in Sec. VI.

G. Bätz, M. Scheint, A. Schmidts and D. Wollherr are with the Institute of Automatic Control Engineering, Technische Universität München, D-80290 München, Germany. E-mail: georg.baetz@tum.de

U. Mettin and A. Shiriaev are with the Department of Engineering Cybernetics, Norwegian University of Science and Technology, NO-7491 Trondheim, Norway.

D. Wollherr is also with the Institute of Advanced Study , Technische Universität München, D-80290 München, Germany.

A. Shiriaev is also with the Department of Applied Physics and Electronics, Umeå University, SE-901 87 Umeå, Sweden.

II. MODELING

This section introduces the hybrid dynamical model that describes periodic motions of a robotic ball-dribbling system. Here, the following assumptions are made:

- A1 The ball and the manipulator are modeled as one-degree-of-freedom (DOF) systems such that only vertical motions are taken into account.
- A2 The ball is modeled as rigid body.
- A3 Impacts between ball and ground are instantaneous inelastic collisions described by the coefficient of restitution c_r. [7]
- A4 Air resistance and rotational ball velocity are negligible.

In the following, the two continuous system dynamics and the overall hybrid dynamics are derived.

A. Coupled Ball-Spring-Manipulator Dynamics

The use of a spring element introduces a continuous-time control phase instead of an instantaneous impact. This modification resembles the human approach where a rather flexible "arm-hand manipulator" is used. The schematic in Fig. 1 shows the 2-DOF ball-spring-manipulator system actuated at the mass m_M. When the ball is in contact with the plate, the system dynamics are given by

$$\begin{aligned} m_M\ddot{x}_M &= u - c\,(x_M - x_B - d_{PB} - l_{c,0}) - m_M g \\ \tilde{m}_B\ddot{x}_B &= c\,(x_M - x_B - d_{PB} - l_{c,0}) - \tilde{m}_B g, \end{aligned} \tag{1}$$

where $\tilde{m}_B = m_B + m_P$ is the merged mass of ball and plate and g the gravitational acceleration. The spring with stiffness c is restricted to its working range $l_c = x_M - x_B - d_{PB}, l_c \in [l_{c,min}, l_{c,0}]$.

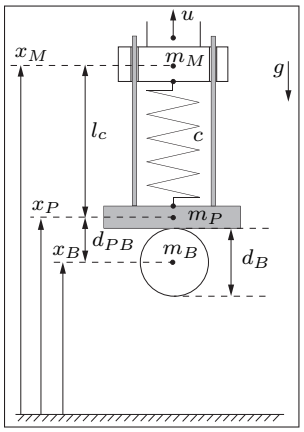

(a) Schematic

Manipulator	m_M = 2 kg m_P = 1 kg
Ball	m_B = 0.62 kg d_B = 0.242 m d_{PB} = 0.171 m
Spring	c = 500 N/m $l_{c,0}$ = 0.157 m $l_{c,min}$ = 0.023 m
Gravitational constant	g = 9.81 m/s^2

(b) Physical Parameters

Fig. 1: Underactuated 2-DOF ball-spring-manipulator system

B. Decoupled Dynamics

For simplicity, we assume that manipulator and plate are rigidly connected when the ball is not in contact with the plate. In practice this can be realized by an electro-mechanical lock. This assumption yields to the following dynamics during free flight

$$\begin{aligned} \tilde{m}_M \ddot{x}_M &= u - \tilde{m}_M g \\ \ddot{x}_B &= -g, \end{aligned} \tag{2}$$

where $\tilde{m}_M = m_M + m_P$ is the merged mass of manipulator and plate.

C. Hybrid Dynamics

The cyclic ball dribbling task is of hybrid nature consisting of continuous phases c (catch), p (push) and f (free flight) separated by instantaneous transitions. The state of the system is given by

$$\boldsymbol{x} = [x_M \;\; x_B \;\; \dot{x}_M \;\; \dot{x}_B]^T \tag{3}$$

and the dynamic model for phase $i \in \{c, p, f\}$ is

$$\dot{\boldsymbol{x}}_i = \boldsymbol{f}_i(\boldsymbol{x}_i, u_i). \tag{4}$$

Here, phases p and c are described by (1), and phase f is described by (2). Switching surfaces S_i^j determine the occurrence of a transition from phase i to j. For such a transition, a reset map can be written as

$$\boldsymbol{x}_j^+ = \Delta_i^j\left(\boldsymbol{x}_i^-\right) \quad \text{for} \quad \boldsymbol{x}_i^- \in S_i^j \tag{5}$$

where $\boldsymbol{x}_i^-$ is the state directly before the transition, $\boldsymbol{x}_j^+$ is the state directly after the transition, and $(i,j) \in \{(f,c),(c,p),(p,f),(f,f)\}$.

The hybrid model of the complete system is obtained by combining equations (4) and (5):

$$\Sigma : \begin{cases} \dot{\boldsymbol{x}}_i = \boldsymbol{f}_i(\boldsymbol{x}_i, u_i) & \boldsymbol{x}_i^- \notin S_i^j \\ \boldsymbol{x}_j^+ = \Delta_i^j\left(\boldsymbol{x}_i^-\right) & \boldsymbol{x}_i^- \in S_i^j \end{cases} \tag{6}$$

with $(i,j) \in \{(f,c),(c,p),(p,f),(f,f)\}$. A summary of discrete states and transitions for a ball dribbling cycle is given in Fig. 2.

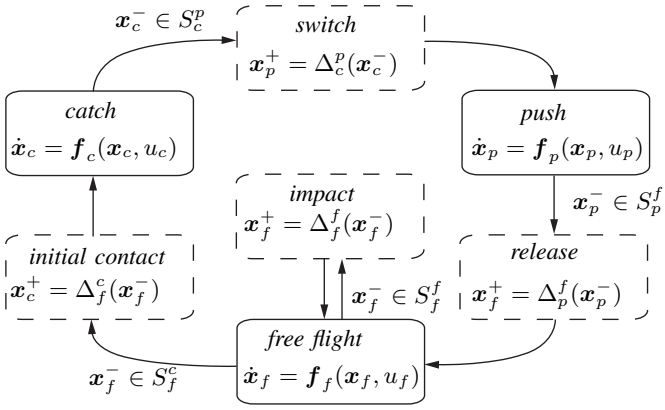

(a) Evolution chart

Switching surface	Reset map
$S_c^p = \dot{x}_B$	$\boldsymbol{x}_p^+ = \Delta_c^p(\boldsymbol{x}_c^-) = \boldsymbol{x}_c^-$
$S_p^f = x_M - x_B - d_{PB} - l_{c,0}$	$\boldsymbol{x}_f^+ = \Delta_p^f(\boldsymbol{x}_p^-) = \boldsymbol{x}_p^-$
$S_f^f = x_B - d_B/2$	$\boldsymbol{x}_f^+ = \Delta_f^f(\boldsymbol{x}_f^-) = [1\ 1\ 1\ -c_r]^T \boldsymbol{x}_f^-$
$S_f^c = x_M - x_B - d_{PB} - l_{c,0}$	$\boldsymbol{x}_c^+ = \Delta_f^c(\boldsymbol{x}_f^-) = = \begin{bmatrix} \boldsymbol{I}_3 & \boldsymbol{0}_{3x1} \\ 0\ 0 & \frac{m_P}{\tilde{m}_B}\ \frac{m_B}{\tilde{m}_B} \end{bmatrix} \boldsymbol{x}_f^-$

(b) Switching surfaces and reset maps

Fig. 2: States and transitions of the hybrid ball dribbling system. Solid boxes depict discrete states, dashed boxes depict instantaneous transitions.

The ball dynamics between release and the subsequent initial contact are not directly controlled. Hence, an algebraic relation for the state of the ball can be derived by integrating (2), see [8]. Furthermore, one can assume that the manipulator dynamics are fast enough to reach the desired state at *initial contact*, starting from *release* during the time that the ball falls to the ground and bounces back. For system analysis, it makes sense to consider only the controlled phase of the ball dribbling cycle involving the dynamics of the underactuated ball-spring-manipulator system (1). The time from *release* to ground *impact* is given by

$$t_f^f - t_p^f = (1/g)\left(\dot{x}_{B,p}^- + \sqrt{(\dot{x}_{B,p}^-)^2 + 2g(x_{B,p}^- - d_B/2)}\right). \tag{7}$$

The ball velocity after the ground impact can be described as function of the ball state at *release* or at *initial contact*:

$$\begin{aligned} \dot{x}_{B,f}^+ &= c_r\sqrt{(\dot{x}_{B,p}^-)^2 + 2g(x_{B,p}^- - d_B/2)} \\ \dot{x}_{B,f}^+ &= \sqrt{(\dot{x}_{B,c}^+)^2 + 2g(x_{B,c}^+ - d_B/2)}. \end{aligned} \tag{8}$$

Using (7) and (8), the evolution chart in Fig. 2(a) can be modified by introducing a new mapping from *release* to *initial contact*.

III. MOTION PLANNING

During the ball-dribbling-cycle there are two continuous phases that provide control over the ball, namely *catch* and *push*. The desired continuous-time motion of the ball-spring-manipulator system (1) can be described by the time evolution of its generalized coordinates

$$\{x_M = x_{M^*}(t),\ x_B = x_{B^*}(t)\},\ \ t \in [t_b, t_e],\ t_b < t_e. \tag{9}$$

However, the facts that the dynamical system (1) is underactuated and the overall system (6) is of hybrid nature poses a challenge for the planning of desired motions.

A. Virtual Holonomic Constraints

By introducing a set of geometric relations among the general coordinates, the motion of (9) can be rewritten as

$$\{x_M = \phi_1(\theta),\ x_B = \phi_2(\theta)\},\ \ \theta = \theta_*(t),\ t \in [t_b, t_e] \quad (10)$$

with a scalar variable $\theta \in [\theta_b, \theta_e]$ that is used as trajectory generator for parameterizing the time evolution. Geometric functions among the generalized coordinates as introduced by (10) are known as *virtual holonomic constraints* [9], [10]. A convenient choice for our system is the following:

$$\begin{bmatrix} x_M \\ x_B \end{bmatrix} := \Phi(\theta) = \begin{bmatrix} \phi(\theta) \\ \theta \end{bmatrix}. \quad (11)$$

Suppose that there exists a control law u_* for the input force u that makes the virtual holonomic constraint (11) invariant, then the overall closed-loop system can be generally represented by reduced order dynamics of the form [9]

$$\alpha(\theta)\ddot{\theta} + \beta(\theta)\dot{\theta}^2 + \gamma(\theta) = 0. \quad (12)$$

The solutions of this virtually constrained system define achievable motions with precise synchronization given by (11). It means the whole motion is parameterized by the evolution of the chosen configuration variable θ. The smooth coefficient functions of (12) can be derived from the system dynamics (1) substituting (11):

$$\begin{aligned} &\alpha(\theta) = \tilde{m}_B, \qquad \beta(\theta) = 0 \\ &\gamma(\theta) = -c\left(\phi(\theta) - \theta - d_{PB} - l_{c,0}\right) + \tilde{m}_B g. \end{aligned} \quad (13)$$

The reduced order dynamics of the form (12) is always integrable. Specifically, the integral function [9]

$$I(\theta_b, \dot{\theta}_b, \theta, \dot{\theta}) = \dot{\theta}^2 - \dot{\theta_b}^2 + \int_{\theta_b}^{\theta} \frac{2\gamma(s)}{\alpha(s)} ds \quad (14)$$

preserves its zero value along the solution of (12), initiated at $[\theta_b(t_b), \dot{\theta_b}(t_b)] = [\theta_b, \dot{\theta_b}]$.

With the above arguments, the motion planning problem can be converted from a search of feasible orbits in the state space into a search for a parameterizing function $\phi(\theta)$ such that a desired solution of the reduced dynamics is found. Here, a Bézier polynomial [10]

$$\phi(\theta) = \sum_{k=0}^{M} a_k \binom{M}{k} s^k (1-s)^{M-k}, \qquad s = \frac{\theta - \theta_b}{\theta_e - \theta_b} \quad (15)$$

is used as geometric relation between the generalized coordinates. Hence, one needs to find the coefficients $\boldsymbol{a} = [a_0 \dots a_M]$ that lead to the desired time evolution $\theta_*(t)$ between the specified initial and final conditions $[\theta_b, \dot{\theta}_b, \theta_e, \dot{\theta}_e]$.

B. Trajectory Optimization

For the trajectory optimization, the following restrictions are considered: At the beginning of the catching phase and at the end of the pushing phase, we constrain the spring to be at equilibrium length. Furthermore, the condition of continuity requires $\boldsymbol{x}_p^+ = \Delta_c^p(\boldsymbol{x}_c^-) = \boldsymbol{x}_c^-$. With these requirements, the Bézier coefficients $a_0^{(c)}$, $a_0^{(p)}$ and $a_M^{(p)}$ are fixed. Optimization is used to determine the remaining coefficients $\boldsymbol{a}^{(c)}$ and $\boldsymbol{a}^{(p)}$ of the Bézier polynomials for the *catching* and the *pushing* phase. The nonlinear optimization problem is defined as

$$\begin{aligned} &\min_{\boldsymbol{\gamma} \in \Gamma} \quad J_i(\boldsymbol{\gamma}) \\ &\text{with} \quad \Gamma = \left\{\boldsymbol{\gamma} \in \mathbb{R}^{2M-1}, \boldsymbol{c}_i(\boldsymbol{\gamma}) \le \boldsymbol{0}, c_e(\boldsymbol{\gamma}) = 0\right\} \\ &\qquad \boldsymbol{\gamma} = \left[a_1^{(c)} \dots a_M^{(c)}, a_1^{(p)} \dots a_{M-1}^{(p)}\right] \end{aligned} \quad (16)$$

The inequality constraints $\boldsymbol{c}_i(\boldsymbol{\gamma})$ originate from the limitations of the physical system, such as maximum actuator acceleration and limits of the spring deflection. The equality constraint $c_e(\boldsymbol{\gamma})$ ensures the validity of the reduced order dynamics.

$$\boldsymbol{c}_i(\boldsymbol{\gamma}) = \begin{bmatrix} ||u(\boldsymbol{\gamma})||_2 - a_{max} \\ (x_M(\boldsymbol{\gamma}) - x_B - d_{PB}) - l_{c,0} \\ l_{c,min} - (x_M(\boldsymbol{\gamma}) - x_B - d_{PB}) \end{bmatrix} \quad (17)$$

$$c_e(\boldsymbol{\gamma}) = I(\theta_b, \dot{\theta}_b, \theta, \dot{\theta}, \boldsymbol{\gamma}) \quad (18)$$

Two different cost functions are considered for the trajectory optimization. The function J_1 evaluates the maximum manipulator velocity and J_2 estimates the energy consumption:

$$\begin{aligned} J_1(\boldsymbol{\gamma}) &= \lambda \ \max ||\dot{x}_M(t)||_2^2 + e(t_e) \\ J_2(\boldsymbol{\gamma}) &= \frac{\lambda}{T} \int_{t_s}^{t_e} u(t)^2 dt + e(t_e). \end{aligned} \quad (19)$$

with $\lambda = 10^2$, $T = t_e - t_b$ and the terminal cost

$$e(t_e) = \lambda_v e_v(t_e)^2 + \lambda_p e_p(t_e)^2 \quad (20)$$

which punishes deviations of the final velocity and position ($\lambda_v = \lambda_p = 10^6$) at the end of each phase. Based on these cost functions, trajectory optimization has been performed for different degrees of the Bézier polynomial (15). For the optimization results in this paper, a particular ball dribbling cycle is considered: The desired dribbling height is set to $h_d = x_{B,c}^- = x_{B,p}^+ = 0.9$ m, the *initial contact* to $[x_{B,c}^+, \dot{x}_{B,c}^+] = [0.8\text{ m}, 1.72\text{ m/s}]$ m and the *release* to $x_{B,p}^- = x_{B,f}^+ = 0.5$ m is considered. With a known coefficient of restitution c_r, the ball velocity $\dot{x}_{B,p}^-$ at release is determined with the two equations from (8). Table I summarizes the results of the numerical optimization with *fmincon* from MATLAB. For both cost functions, the higher order Bézier polynomials naturally lead to reduced costs. However, there is no significant difference in the costs between $M = 5$ and $M = 6$. Hence, a Bézier polynomial of order $M = 5$ is a good trade-off between cost optimality and numerical complexity, which is relevant for the implementation on the real system. For comparison, Fig. 3 shows optimized trajectories and the resulting spring deflection for $M = 3$ and $M = 5$ obtained when using J_1.

Bézier Degree	J_1	J_2
3	779.208	80249
4	719.756	77663
5	707.964	75234
6	706.043	74134

TABLE I: Costs of the optimized trajectories for different Bézier degrees

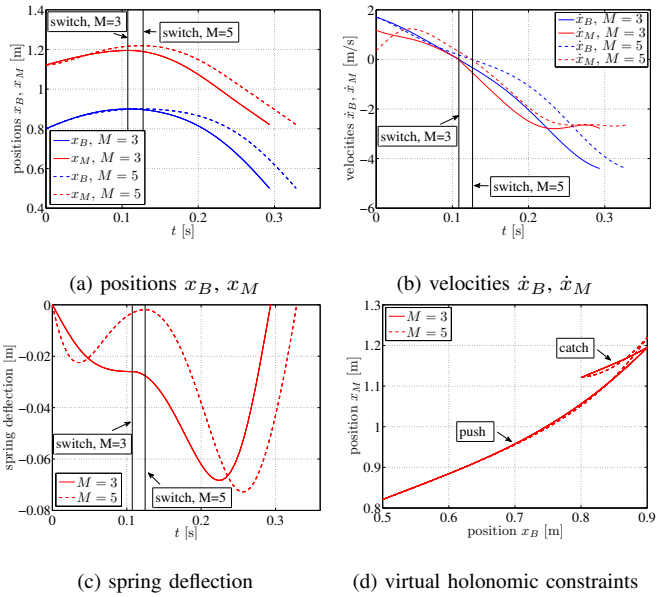

(a) positions x_B, x_M (b) velocities $\dot{x}_B$, $\dot{x}_M$

(c) spring deflection (d) virtual holonomic constraints

Fig. 3: Optimized trajectories for different Bézier degrees using cost function J_1. The solid lines indicate the switch from *catch* to *push* phase.

IV. CONTROL DESIGN

A. Transverse Linearization

Given the desired orbit obtained through the optimization process, the next step is to design a controller that stabilizes the ball-spring-manipulator system in the vicinity of the desired trajectory. Based on the system description in the form of (10), new coordinates and velocities are introduced in the vicinity of the target orbit:

$$\begin{aligned} x_M &= \phi(\theta) + y, & x_B &= \theta \\ \dot{x}_M &= \phi'(\theta)\dot{\theta} + \dot{y}, & \dot{x}_B &= \dot{\theta}. \end{aligned} \tag{21}$$

The dynamics of the synchronization error y to the specified virtual holonomic constraint can be computed from the system dynamics (1) by substituting (21):

$$\ddot{y} = r(\theta, \dot{\theta}, y, \dot{y}) + (1/m_M)\, u = v. \tag{22}$$

An auxiliary control signal v is introduced by a control transformation via partial feedback linearization [11]. The dynamics of θ is given by substituting (21) into the second order differential equation (12), which yields

$$\tilde{m}_B\ddot{\theta} - c\,(\phi(\theta) - \theta - d_{PB} - l_{c,0}) + \tilde{m}_B g = -cy, \tag{23}$$

where the right hand side equals to zero on the desired orbit. The target motion (9) in the new generalized coordinates is given by

$$\{y_*(t) \equiv 0, \quad \theta = \theta_*(t)\}, \qquad t \in [t_b, t_e]. \tag{24}$$

The dynamic system has a natural choice of transverse coordinates $x_\perp = [I(\theta, \dot{\theta}, \theta_{b*}, \dot{\theta}_{b*}) \;\; y \;\; \dot{y}]^T$ that describe the system's behavior away from a specified orbit [9]. We can analytically compute a transverse linearization along a continuous-time target motion (24) to be used for system analysis and control design:

$$\begin{aligned} \frac{d}{d\tau} z &= A(\tau)z + BV = \\ &= \begin{bmatrix} 0 & \frac{2\dot{\theta}_*(\tau)}{\tilde{m}_B} c & 0 \\ 0 & 0 & 1 \\ 0 & 0 & 0 \end{bmatrix} \begin{bmatrix} I \\ Y_1 \\ Y_2 \end{bmatrix} + \begin{bmatrix} 0 \\ 0 \\ 1 \end{bmatrix} V. \end{aligned} \tag{25}$$

A cyclic solution $z = z(\tau) = z(\tau + T)$ with time period $T = t_p^f - t_f^c$ and a switch at $T_s = t_c^p$ is defined by:

$$\begin{aligned} \frac{d}{d\tau} z &= A(s)z + BV, \qquad s = \tau \bmod T \\ A(s) &= \begin{cases} A_c(s), s \in (0, T_s] \\ A_p(s), s \in (T_s, T) \end{cases} \\ z(\tau_{k+}) &= F z(\tau_{k-}), \quad \tau_k = kT, \quad k \in \mathbb{N}. \end{aligned} \tag{26}$$

The operator F is mapping from *release* to *initial contact*.

B. Closed-Loop System

Consider the control law

$$V = K(s)z, \qquad K(s) = \begin{cases} K_c(s), s \in (0, T_s] \\ K_p(s), s \in (T_s, T) \end{cases} \tag{27}$$

for the hybrid linear system (26). It can be shown that exponential stability of the origin for the linear impulsive system is equivalent to exponential orbital stability of the periodic motion for the nonlinear one [12]. For reasons of implementation only a constant feedback of the synchronization error $x_M - \phi(x_B)$ shall be used since these measurements are available:

$$K_c = [0, k_c, 0], \qquad K_p = [0, k_p, 0]. \tag{28}$$

In addition to the control during the two contact phases *catch* and *push*, one has to apply a control for the manipulator during the non-contact phase. This control law has to ensure that the manipulator is at the desired state when the controlled phase of the ball dribbling cycle starts.

C. Overall Control Structure

The overall control structure of the system is depicted in Fig. 4. It has three main modules: ball tracking, ball trajectory prediction and robot trajectory generation. In the first module, ball tracking is performed based on visual sensor information. In the second module, the ball trajectory is predicted based on the provided sensor feedback. In the third module, the end effector trajectory is generated based on the tracked/predicted ball trajectory. For the motion control of the robot, a computed torque feed forward control in combination with a decentralized PD-controller is used [13].

V. EXPERIMENT & RESULTS

This section introduces the experimental setup and presents the results of two experiments: First, a dribbling task performed by a human is evaluated. Second, robotic dribbling with vision sensor based feedback is evaluated.

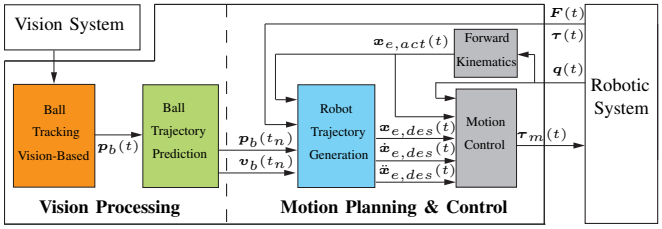

Fig. 4: Overall control structure

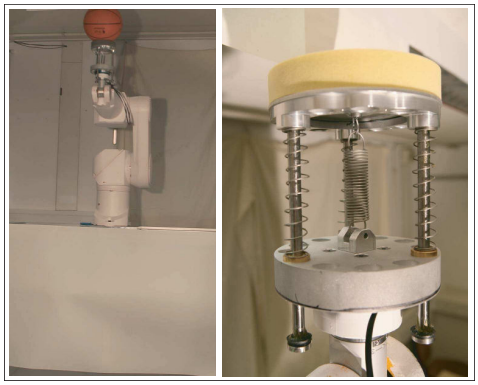

Fig. 5: Six DoF robot with the spring-manipulator system used as end effector

A. Experimental Setup

1) Robotic System: For the experiments, a Stäubli RX90B industrial robot with six revolute joints is used. In order to implement and evaluate own control concepts, a PC-based controller works in parallel with the robot control unit. The configuration, calibration and supervising of the robot is performed with the original architecture. The control is passed over to the additional PC, which runs Matlab/Simulink in a real-time Linux (RTAI) environment.

2) End Effector: The robot is equipped with a 6-DOF force/torque sensor and a circular plate with radius 0.07 m is used as end effector. The plate is attached to the robot through an elastic coupling which allows relative motion between plate and robot. Fig. 5 shows the robot and the spring-manipulator system.

3) Vision System: The stereo vision system for object tracking consists of two Mikrotron MC1311 high-speed cameras, two frame grabbers and a general purpose PC with two PCIe ports. The tracking algorithm obtains images from the frame grabber for image processing. The ball position is sent to the control PC via a TCP network connection. The two cameras are mounted with a baseline b = 2 m and converging axes. The distance between baseline and fixation point is 3 m, and between baseline and robot base 3.5 m. For details on the ball tracking algorithm see [8].

B. Reduced Mechanical Load

The use of a mechanical spring element promises to reduce the mechanical load on the end effector. In order to evaluate this assumption, the following experiment was conducted: a basketball impacted the end effector with a relative velocity of 1.4 m$/$s and the resulting contact forces at the manipulator

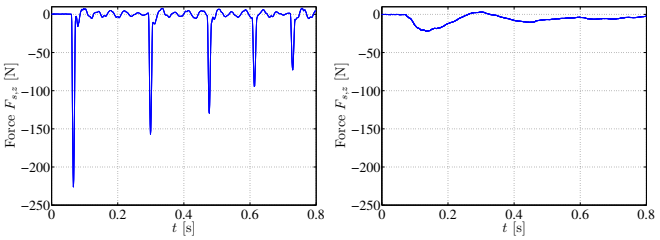

(a) intermittent contact (b) continuous-time contact phase

Fig. 6: Measured impact forces for (a) intermittent contact and (b) continuous-time contact phase

were recorded. Fig. 6(a) shows the contact force for a rigid end effector design: During the initial impact, the force exceeds 220 N. The ball then rebounces on the end effector, leading to successive impacts. In contrast, Fig. 6(b) shows the contact force for the compliant end effector design: Here, the maximum force is significantly reduced (appr. 25 N). In addition, the compliant structure leads to a continuous contact phase after the initial impact.

C. Dribbling With Vision Sensor Based Ball Tracking

1) Initialization: The dribbling task can be initialized either by the robot or the human operator. In the former case, which was used for the experiments, the ball is initially at rest on the plate and then dropped by the robot to start the dribbling cycle. Fig. 7 illustrates this *autonomous* initialization. In the latter case, the task is triggered when the ball is dropped into a specified area of the robot workspace.

2) Dribbling Cycle: The desired initial and final states for the experimentally studied dribbling cycle are summarized in Table II. For the experiment, a constraint for the relative velocity between ball and manipulator at the time of initial contact is added:

$$\dot{x}^{+}_{M,c} = 0.95\ \dot{x}^{+}_{B,c}. \tag{29}$$

The coefficient of restitution of the ball was experimentally determined to be $c_r = 0.84$. During the dribbling cycle, the ball position is tracked by the vision system. For the contact phases *catch* and *push*, the control law described in Sec. IV.B. is used. During the non-contact phase the robot trajectory is generated and updated based on the tracked ball position and the predicted impact time. For all phases, an additional controller is used to compensate horizontal deviations, see [8] for details. Fig. 8 shows the actual manipulator and ball position in vertical direction during a dribbling experiment. The ball trajectory starts at 0.75 s when the ball is detected by the vision system. A snapshot sequence of the initialization and the first dribbling cycle is depicted in Fig. 7. Currently, the performance is mainly limited by the following aspect: In the simulation, it was assumed that there is no energy loss in the elastic actuator. For the real actuator however, friction forces during spring compression/elongation cause energy dissipation. This, in turn, leads to a reduced amount of energy storage in the spring and energy transfer to the ball.

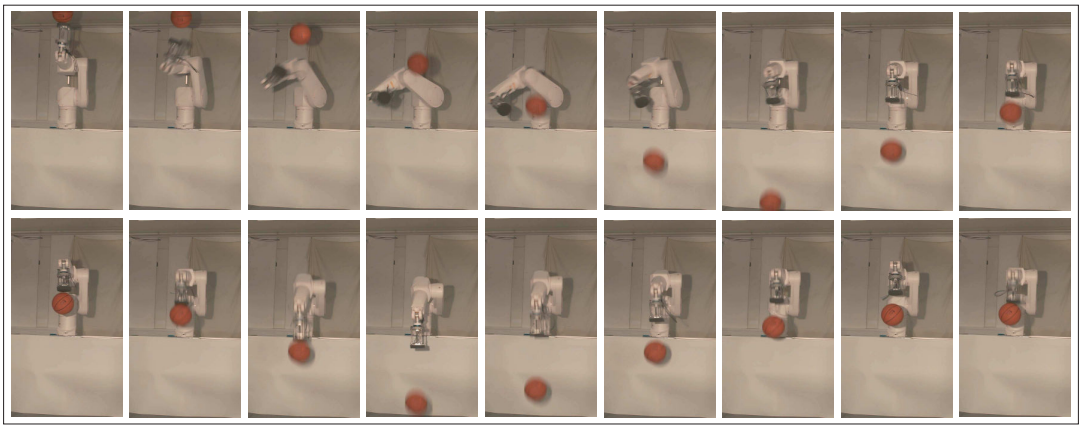

Fig. 7: Snapshots of the task initialization and the first dribbling cycle (sequence from 0 s to 2.16 s, time duration between two snapshots: 0.12 s)

	initial contact	*switch*	*release*
x_M [m]	1.605	1.65*	1.285
x_B [m]	1.32	1.38	1.00
$\dot{x}_M$ [m/s]	1.1438	0	-2.91*
$\dot{x}_B$ [m/s]	1.204	0	-4.26

TABLE II: Initial and final states for the experimentally studied dribbling cycle. Entries marked with * are obtained through trajectory optimization

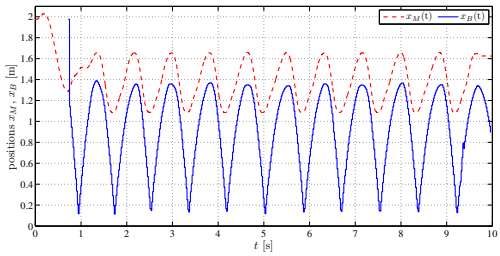

Fig. 8: Actual manipulator and ball position in vertical direction for a dribbling sequence of ten cycles.

VI. CONCLUSION

A novel approach for the stabilization of human-like periodic ball dribbling motion was presented. Adding an elastic element to the manipulator offers two benefits: First, the ball can be controlled in a continuous-time phase instead of an intermittent contact. Second, impacts between manipulator and ball are avoided which reduces the mechanical load. The virtual holonomic constraints approach was used to plan optimal catching and pushing trajectories considering two different cost functions. An orbitally stabilizing feedback controller was designed for the underactuated ball-spring-manipulator system based on a transverse linearization along the desired motion. Numerical simulations and first experiments have been conducted to evaluate the control design. Experimental results showed that the new approach reduces the contact forces by avoiding hard impacts, which lowers the mechanical load for the manipulator. In addition, first dribbling experiments have been conducted to validate the approach. Future research will further investigate the trajectory optimization: a simultaneous optimization of spring constant and Bézier coefficient is likely to lead to reduced costs. In addition, the use of a spring with nonlinear characteristic will also be considered. Further experiments will be conducted to evaluate the new approach and compare it to control strategies based on intermittent contact.

VII. ACKNOWLEDGMENTS

The authors would like to thank Haiyan Wu and Kolja Kühnlenz for their valuable contributions. The first author gratefully thanks the German National Academic Foundation for their support.

REFERENCES

[1] M. Bühler, D. Koditschek, and P. Kindlmann, "A family of robot control strategies for intermittent dynamical environments," *IEEE Control Systems Magazine*, vol. 10, pp. 16–22, Feb. 1990.

[2] P. J. Holmes, "The dynamics of repeated impacts with a sinusoidally vibrating table," *Journal of Sound and Vibration*, vol. 84, no. 2, pp. 173 – 189, 1982.

[3] M. Bühler, D. Koditschek, and P. Kindlmann, "Planning and control of robotic juggling and catching tasks," *The International Journal of Robotics Research*, vol. 13, no. 2, pp. 101 – 118, 1994.

[4] K. M. Lynch and C. K. Black, "Recurrence, controllability and stability of juggling," *IEEE Transaction on Robotics and Automation*, vol. 17, no. 2, pp. 113 – 124, 2001.

[5] D. Shiokata, A. Namiki, and M. Ishikawa, "Robot dribbling using a high-speed multifingered hand and a high-speed vision system," in *Proc. IEEE International Conference on Intelligent Robots and Systems (IROS)*, 2005.

[6] G. Bätz, M. Sobotka, D. Wollherr, and M. Buss, "Robot basketball: Ball dribbling - a modified juggling task," in *Advances in Robotic Research - Theory, Implementation, Application* (T. Kröger and F. M. Wahl, eds.), Springer, 2009.

[7] A. Domenech, "A classical experiment revisited: The bounce of balls and superballs in three dimensions," *American Journal of Physics*, vol. 1, pp. 28 – 36, 2005.

[8] G. Bätz, K.-K. Lee, D. Wollherr, and M. Buss, "Robot basketball: A comparison of ball dribbling with visual and force/torque feedback," in *IEEE International Conference on Robotics and Automation*, 2009.

[9] A. Shiriaev, L. Freidovich, and S. Gusev, "Transverse linearization for controlled mechanical systems with several passive degrees of freedom," *IEEE Transactions on Automatic Control*, vol. 55, pp. 1–13, 2010.

[10] E. Westervelt, J. Grizzle, C. Chevallereau, J. Choi, and B. Morris, *Feedback Control of Dynamic Bipedal Robot Locomotion*. CRC Press, Taylor & Francis Group, 2007.

[11] M. W. Spong, "Partial feedback linearization of underactuated mechanical systems," in *Proceedings of the IEEE/RSJ/GI International Conference on Intelligent Robots and Systems (IROS)*, 1994.

[12] A. Shiriaev, L. Freidovich, and I. Manchester, "Periodic motion planning and analytical computation of transverse linearizations for hybrid mechanical systems," in *Proc. 47th IEEE Conference on Decision and Control*, 2008.

[13] B. Siciliano, L. Sciavicco, L. Villani, and G. Oriolo, *Robotics - Modelling, Planning and Control*. Springer, 2008.